Classification
Physics Abstracts
61.12 — 87.15 — 36.20

Partial and charge structure functions of monodisperse DNA fragments in salt free aqueous solution

J. R. C. van der Maarel (1), L. C. A. Groot (1), M. Mandel (1), W. Jesse (1), G. Jannink (2) and V. Rodriguez (3)

(1) Department of Physical and Macromolecular Chemistry, Gorlaeus Laboratories, Leiden University, P. O. Box 9502, 2300 RA Leiden, The Netherlands
(2) Laboratoire Léon Brillouin (*), CEN-Saclay, 91191 Gif-sur-Yvette Cedex, France
(3) Institute von Laue-Langevin, 156X, 38042 Grenoble Cedex, France

(*Received 12 July 1991, revised 18 September 1991, accepted 27 September 1991*)

Résumé. — On reconstitue la structure d'une solution aqueuse de fragments monodisperse d'ADN à l'aide des fonctions de structure partielles et de la fonction de structure de charge mesurées par diffusion des neutrons aux petits angles. Dans l'intervalle $q \geq 0{,}075$ Å^{-1}, les fonctions de corrélation calculées à partir de la solution exacte de l'équation de Poisson-Boltzmann et du modèle cellulaire, ajustent les données de l'expérience. Cela est vrai aussi bien pour chacune des fonctions de structure partielles que pour la fonction de structure de charge. Le modèle cellulaire semble donc être un modèle convenable pour ces solutions.

Abstract. — Observations of the partial structure functions and the charge structure function are reported for an aqueous solution of monodisperse rodlike DNA fragments, without added simple salt. In the reciprocal space interval $q \geq 0.075$ Å^{-1}, the neutron scattering data can be fitted by the correlation functions derived from the exact solution of the Poisson-Boltzmann equation in the cell model. The fit is equally good for all partial structure functions as well as the charge structure function. The cell model seems to be appropriate for this kind of solution.

1. Introduction.

The spatial distribution of charges in aqueous solution is a problem of general interest, related to the effects of the Coulomb interaction. This problem is theoretically difficult to assess due to the long range of the interaction. Many experimental observations can, however, be related to these effects. The latter are sensitive to the geometry as determined by the molecular shape and the charge distribution dissymmetry. The purpose of this paper is to give experimental evidence of correlation between charges in aqueous solutions of monodisperse DNA fragments (146 base-pairs, contour length $L = 500$ Å). The counterions are tetramethylammonium (TMA^+) and there is no low molecular weight salt present in solution.

To obtain these results we have measured small angle neutron scattering intensities at

(*) Laboratoire commun CEA-CNRS.

different isotopic compositions of the solvent. The partial structure functions, related to the nucleotides, the counterions, and the cross term, are then derived from the experimental data. In a particular isotopic solvent (H_2O/D_2O) composition for which the average contrast length equals zero, the scattered intensity is proportional to the charge structure function. This function will also be presented here and its significance will be discussed.

There are already several well established experimental results obtained by radiation scattering from aqueous solutions containing charged particles. However, our experiments differ from previous ones in several respects : the aim, the method, and the sample. Until now, in most cases, the experimental evidence is limited to a combination of partial structure functions. This combination tends to be dominated by the monomer-monomer partial structure function [1]. The result then gives important information on the polyion form function and the polyion distinct pair correlation function. However, it does not provide a sufficient description of the system which is in fact characterized by all the partial structure functions. When the weights of the partial structure functions are all comparable, the scattered intensities can be fitted to the combination of model partial structure functions [2]. However, this procedure is not capable of determining each partial structure function separately.

More recently experiments have been performed using contrast variation. From the experimental data all the partial structure functions could be derived. This was done in particular for the case of charged micelles [3] and linear poly-(styrenesulfonate) [4]. The micelles are considered as rigid spheres and in this geometry all the partial structure functions can be calculated in a self-consistent manner using the Ornstein-Zernike formalism. Self-consistency can be demonstrated in the ratios of the different partial structure functions at zero angle. The accumulation of counterions on the spheres could be observed directly. There are however other molecular shapes of interest, in particular the linear or cylindrical geometry.

In the case of linear polyions every charge is associated with a monomer which has a relatively small volume. Moreover, the conformation of linear flexible polyelectrolytes (e.g., poly-(acrylicacid)) depends strongly on charge density and concentration, in contrast to the case of spherical polyions. A self-consistent structure is difficult to model in this case. Linear 146 base-pair DNA fragments are considered as rigid rodlike cylinders ; the intrinsic persistence length is of the order of the contour length as has been demonstrated with the help of light scattering measurements [5]. Tetramethylammonium salts are known to have no significant effect on the stability of the DNA secondary structure [6]. An analysis of the circular dichroism shows the DNA in the presence of TMA^+ counterions to be in the double helix B form. For cylindrical geometry a self-consistent charge distribution can then be predicted on the basis of the solution of the Poisson-Boltzmann equation and the so called cell model [7-9].

In the cell model the diameter of the cell is fixed by the polyion concentration. The radial charge distribution is the relevant quantity. Here it is assumed that positive and negative charges occupy different parts within the cell. This is different from the case of simple electrolytes, for which all ions are distributed over the total volume. For the DNA fragments, it can be argued that each polyion wanders around with its cloud of counterions. The results derived from this model are in agreement with thermodynamic properties of not too concentrated polyelectrolyte solutions, but does it also reflect the true average structure of such systems ? The cell model is of course incomplete, especially at large correlation distances (i.e., small q values). However, we can test in a consistent manner the extent of the q interval within all three partial structure functions can be described by the cell-model and the use of the Poisson-Boltzmann equation.

The solution of the Poisson-Boltzmann equation predicts analytically the counterion distribution in the radial direction away from the polyion axis. This distribution will be tested using the experimentally determined partial structure functions. Because of the high dissymmetry in charge, the counterion-nucleotide cross structure function and the charge structure function are very sensitive to the nature of this radial distribution.

2. Theory.

The solvent contrast matching method has been applied to unravel the measured scattered intensities into the partial structure functions [10]. At low resolution, the solvent contributes an incoherent background which will be subtracted from the measured intensities. Accordingly, the corrected intensity of the neutron radiation scattered by a polyelectrolyte solution (e.g., DNA without added simple salt) reads [11]

$$I(q) = c[\bar{b}_m^2 S_{mm}(q) + 2\bar{b}_m \bar{b}_c S_{mc}(q) + \bar{b}_c^2 S_{cc}(q)]. \quad (1)$$

Here $\bar{b}_m$ and $\bar{b}_c$ are the scattering length contrasts of the monomer and counterion, respectively, and c is the concentration. The monomer-monomer, monomer-counterion, and counterion-counterion partial structure functions are denoted by S_{mm}, S_{mc}, and S_{cc}, respectively. For a H_2O/D_2O solvent mixture, the scattering length contrast $\bar{b}_i$ of the nucleic acid monomers ($i = m$) or counterions ($i = c$) is given by

$$\bar{b}_i = b_i - b_s \bar{v}_i/\bar{v}_s \quad \text{with} \quad b_s = X b_{D_2O} + (1 - X) b_{H_2O} \quad (2)$$

where b_i and b_s are the scattering lengths of the dispersed particle and solvent, respectively. The corresponding partial molal volumes are denoted by $\bar{v}_i$ and $\bar{v}_s$. The dispersed particle scattering length contrast can be adjusted by variation of the D_2O mole fraction X.

The structure functions are calculated theoretically using the cell model [7-9]. The DNA polyion is assumed to be an uniformly charged rod with a length L and a radius r_p. Each molecule is thought to occupy an electroneutral coaxial cell of the same length L but of radius r_{cell}. The cell radius is related to the concentration c (in monomers per unit volume) according to $cA\pi r_{cell}^2 = 1$ with A the mean z-axis projected distance between nucleic acid monomers. The number of nucleotides per DNA molecule is $N = L/A$. The distance of closest approach of the center of mass of the counterions with respect to the polymer is denoted by r_c. Due to the finite size of the counterions, r_c is not necessarily equal to the DNA polymer radius r_p. This will be detailed below. The various geometric parameters are collected in table I.

In the radial direction from the DNA axis the monomer density $\rho_m(r)$ is assumed to be uniform for $0 \leqslant r \leqslant r_p$ and given by $A\rho_m \pi r_p^2 = 1$, and zero for $r > r_p$. The distribution of the counterions within the cell is assumed to be uniform in the longitudinal (z) direction. In the radial direction, this distribution $\rho_c(r)$ is obtained from the analytical solution of the Poisson-Boltzmann equation for an uniformly charged cylinder [8]. The cell model does not necessarily imply an arrangement as arrays of parallel rods. However, a condition is that the electric field should be close to zero in a sufficiently wide range near the cell boundary [9]. Any interactions and/or correlations between different cell volumes (intercellular effects) are neglected. This confines our treatment to sufficiently high values of momentum transfer and/or relatively diluted solutions.

Table I. — *Geometric parameters* 0.099 mole P/l TMA-DNA *solutions.*

L	500 Å	a
r_p	8 Å	b
r_c	14 Å	c
r_{cell}	55.8 Å	d
A	1.71 Å	e
N	292	f
ξ	4.15	g

[a] Fragment length. [b] DNA radius, this work. [c] Distance of closest approach TMA counterions to the rod, this work. [d] Cell radius, determined by concentration. [e] Mean z-axis projected distance between nucleotides. [f] Number of nucleotides per DNA fragment. [g] Linear charge density parameter Q/A, with Q the Bjerrum length (Q = 7.1 Å, 293 K).

For cylindrical geometry and neglect of intercellular effects, the partial structure functions are evaluated in the appendix. The result is given by

$$S_{ij}(q) = \frac{1}{N} \int_0^1 d\mu \left[\frac{\sin(q\mu L/2)}{(q\mu L/2)} \right]^2 P_i(q, \mu) P_j(q, \mu) \tag{3a}$$

with $\mu = \cos(\theta)$, θ being the angle between the momentum vector $\mathbf{q}$ and the z-axis, and

$$P_i(q, \mu) = 2\pi L \int_0^{r_{cell}} dr\, r J_0(qr\sqrt{(1-\mu^2)})\, \rho_i(r) . \tag{3b}$$

Here J_0 is the zero order Bessel function of the first kind and the integration over variable μ follows from the isotropic orientation averaging of the cell volume with respect to $\mathbf{q}$. The radial nucleic acid monomer distribution is assumed to be a step function, and, hence, equation (3b) reduces to (with i = m)

$$P_m(q, \mu) = 2N \frac{J_1(qr_p\sqrt{(1-\mu^2)})}{(qr_p\sqrt{(1-\mu^2)})} \tag{4}$$

Although in the cell model the radial counterion distribution $\rho_c(r)$ is known in analytical form from the solution of the Poisson-Boltzmann equation, the related $P_c(q, \mu)$ has to be evaluated by a numerical integration method. A similar expression, but for X-ray scattering, has been reported in the literature [3].

The charge structure function is defined by [12]

$$S_{zz}(q) = S_{mm}(q) - 2S_{mc}(q) + S_{cc}(q) . \tag{5}$$

With the cell model, this function can be calculated using equation (3) with $i = j = z$ and $\rho_z = \rho_c - \rho_m$. It should be borne in mind that there are only two adjustable parameters : the DNA polymer radius and the distance of closest approach of the counterions to the rod.

In the limit of small values of momentum transfer, for electrolyte solutions there are several sum rules such as the Stillinger and Lovett condition [13]

$$S_{zz}(q) = \frac{2q^2}{\kappa^2}, \qquad q < \kappa \tag{6}$$

with κ^{-1} the Debye screening length. In case of simple electrolytes this length is defined according to $\kappa^2 = 8\pi Qc$, with the Bjerrum length $Q = e^2/\varepsilon kT$. However, in solutions containing polyelectrolytes with a high linear charge density and without added simple salt the true value of the screening length is unknown. In the present contribution, the limiting law equation (6) will be compared to the experimental data using an optimized value of κ.

3. Experimental.

Chicken blood erythrocyte nucleosome DNA was isolated and digested by micrococcal nuclease. The DNA was purified and proteins were removed. For a detailed description of the DNA isolation and characterization the reader is referred to reference [14]. Sodium DNA solutions were extensively dialysed with 0.1 N TMACl against water at 277 K. The exchange of the sodium counterions was monitored using atomic absorption spectroscopy. Excess low molecular weight salt was removed by dialysis and checked by conductivity measurements. Care was taken to avoid contamination with ionic impurities. The circular dichroism spectrum of TMA-DNA at 296 K shows the typical behavior of the B form, i.e., a maximum at 278 nm, a negative minimum at 248 nm, and base-line intersections at 261 and 229 nm [15].

DNA solutions were prepared, in which the H_2O/D_2O solvent composition was chosen according to the experimental specifications. The scattering length contrast parameters have been calculated using equation (2) and the parameters collected in table II. In the calculation of the monomer scattering length contrast, on the average two solvent exchangeable protons per base have been taken into account. The contrast parameters and isotopic composition of the samples are collected in table III. The concentration amounts 0.099 mole P (phosphorus)/l, which corresponds to 5.98×10^{-5} nucleic acid monomers/Å^3.

Neutron scattering experiments were performed using the D17 SANS spectrometer, situated on the cold source of the high flux reactor at the institute von Laue-Langevin, Grenoble. A wave length of 11 Å was selected. The scattered intensity was measured by a planar square multi detector, reaching a maximum q value of 0.37 Å^{-1}. Quartz sample cells with 0.2 cm (for D_2O containing samples) or 0.1 cm path length were used. The temperature was controlled at 293 K. The average counting time per sample (i.e., solution or solvent) was approximately four hours. The data were put on an absolute scale by normalizing to pure

Table II. — *Partial molal volumes and scattering lengths of the various components.*

	$\bar{v}_i$ cm^3/mole	b_i, 10^{-12} cm
nucleotide	172	9.750 + 1.991 X (*)
TMA	84	− 0.890
H_2O	18	− 0.168
D_2O	18	1.915

(*) X denotes the D_2O mole fraction (effect of exchangeable protons). The nucleotide scattering length has been calculated using the values reported by Jacrot [10] and according to the base composition A : G : C : T = 0.288 : 0.205 : 0.215 : 0.292 [17].

Table III. — *Scattering length contrast and isotopic composition* (*).

sample	$\bar{b}_m$, 10^{-12} cm	$\bar{b}_c$, 10^{-12} cm	X, D_2O
s1	11.36	− 0.11	0
s2	4.05	− 4.07	0.408
s3	− 0.01	− 6.27	0.635
s4	−6.42	−9.75	0.993

(*) $c = 5.98 \times 10^{-5}$ nucleic acid monomers/Å^3.

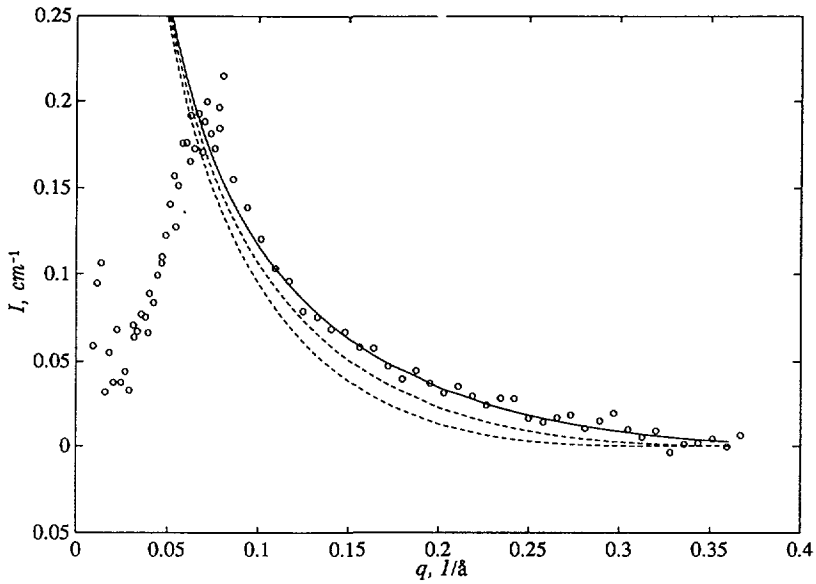

Fig. 1. — Intensity *vs.* momentum transfer : sample s1, 0 % D_2O. The full and dashed curves are drawn according to the cell model calculations with r_c = 14 Å and a DNA polymer radius r_p of 8, 10, and 12 Å from top to bottom.

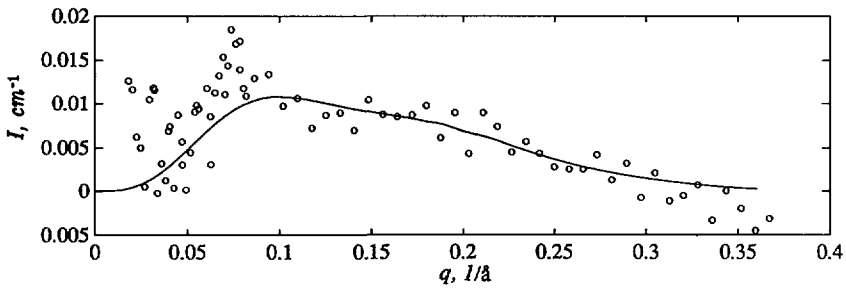

Fig. 2. — Intensity *vs.* momentum transfer : sample s2, 40.8 % D_2O. The solid curve is drawn according to the cell model calculation with r_c = 14 Å and r_p = 8 Å.

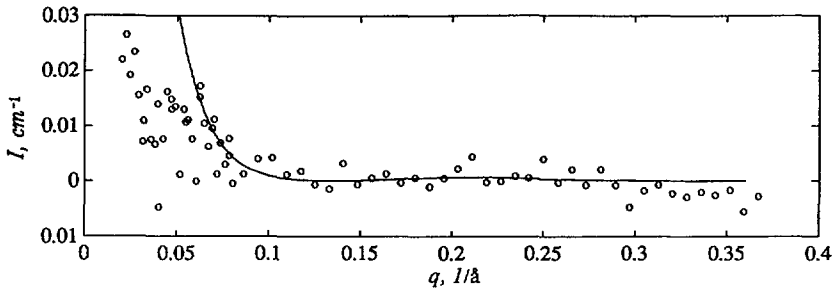

Fig. 3. — Intensity *vs.* momentum transfer : sample s3, 63.5 % D_2O. The solid curve is drawn according to the cell model calculation with $r_c = 14$ Å and $r_p = 8$ Å.

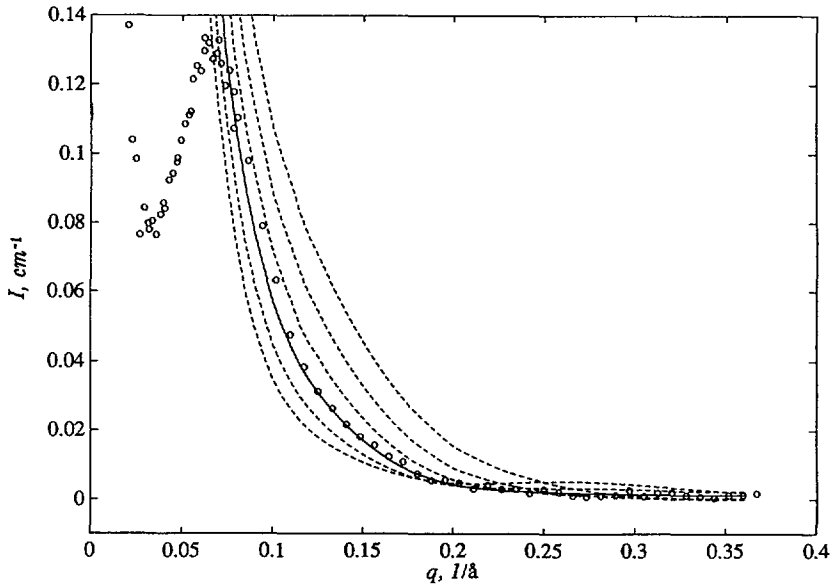

Fig. 4. — Intensity *vs.* momentum transfer : sample s4, 99.3 % D_2O. The full and dashed curves are drawn according to the cell model calculations with $r_p = 8$ Å and distance of closest approach of the counterions to the rod r_c of 8, 10, 12, 14, 16, and 18 Å from top to bottom.

H_2O [16] and the scattering of the pure solvent at the same isotopic H_2O/D_2O composition was subtracted. Finally, the intensities were corrected for a small solute incoherent scattering contribution. The scattered intensity of the four samples as a function of momentum transfer are displayed in figures 1-4, respectively. At very low q values ($q < 0.02$ Å^{-1}) the intensity increases with decreasing q, more or less proportionally to the D_2O mole fraction. Similar behavior has been observed in solutions of the synthetic polyelectrolyte poly-(styrenesulfonate). At present, an explanation can not be given. However, the results at higher values of momentum transfer (the part which will be used in this study) are assumed not to be influenced by this effect.

4. Results and discussion.

According to table III, the counterion scattering length contrast for sample s1 is approximately zero. The measured intensity is directly proportional to the monomer-monomer

partial structure function. For sample s2, the scattering length contrasts have approximately the same magnitude, but opposite signs. In this situation of zero average contrast the scattered intensity is proportional to the charge structure function defined by equation (5). In case of sample s3, the nucleotide scattering length contrast is approximately zero. Now, the intensity is proportional to the counterion-counterion partial structure function. Finally, for sample s4 both scattering length contrast parameters have a sizable value, resulting in a relatively intense scattering.

As mentioned before, the cell model has two adjustable parameters, i.e. the polymer radius r_p and the distance of closest approach of the counterions to the rod r_c. The scattered intensities of the four samples have been calculated with this model and are displayed in figures 1-4. For sample s1, the intensity is nearly completely due to the scattering of the polymer. The counterion contribution is negligible. Accordingly, the polymer radius can be estimated from a comparison of the experimental data to our model calculations. Figure 1 displays the calculated intensities with $r_p = 8$, 10, and 12 Å, together with the geometric parameters collected in table I. For the sake of completeness, the negligibly small counterion contribution has been included with $r_c = 14$ Å (see below). For $q \geq 0.075$ Å^{-1} and $r_p = 8$ Å there is excellent agreement between the experimental data and the calculated curves. The discrepancy at lower values of momentum transfer is clearly due to intermolecular correlations. These intermolecular effects are very difficult to take into account and have been neglected in the model calculations. The value of r_p is somewhat smaller than half of the outer DNA diameter (10 Å, B form [17]). This may be due to the fact that the DNA molecule has an open structure (shallow and deep groove), whereas the model assumes an uniform rod.

After the evaluation of the polymer radius, the distance of closest approach of the counterions to the polymer backbone may be estimated. This is most conveniently performed using the relatively intense scattering of sample s4. Figure 4 displays the calculated intensities using $r_p = 8$ Å and $r_c = 8$, 10, 12, 14, 16, and 18 Å. For $q \geq 0.075$ Å^{-1} and $r_c = 14$ Å there is excellent agreement with the experimental data. This distance of closest approach agrees reasonably with the sum of the TMA ion radius (3.5 Å, [18]) and the outer radius of the DNA molecule (10 Å).

Using the geometric values collected in table I, the intensities of samples s2 and s3 have been calculated too (Figs. 2 and 3, respectively). For sample s3 there is excellent agreement at sufficiently high values of momentum transfer. The discrepancy at small values of q is, again, due to intercellular effects, which have been neglected. In case of sample s2, the correspondence even extends to small q values. It should be borne in mind that the data are on an absolute scale, without the introduction of arbitrary scaling factors to match the theoretical curves.

With equation (1) and the contrast length parameters, from samples s1, s3, and s4, the three partial structure functions S_{mm}, S_{mc}, and S_{cc} are evaluated. The structure functions are assumed to be independent on the solvent isotopic composition. They are displayed in figures 5-7, together with the model calculations. Of course, apart from a scaling factor given by the concentration and the contrast, the monomer-monomer and the counterion-counterion structure functions are similar to the experimental intensities of samples s1 and s3, respectively. The counterion-counterion structure function is approximately equal to zero for $q \geq 0.1$ Å^{-1} The derived monomer-counterion cross partial structure function (Fig. 6) shows a minimum corresponding to a negative value of the structure function at a momentum transfer $q \approx 0.2$ Å^{-1} This is due to the shell-like clustering of the counterions about the polyion. Moreover, the position of this minimum is highly sensitive to the value of r_c (see Fig. 6). Again, the discrepancy at small values of q is due to the neglect of intercellular effects.

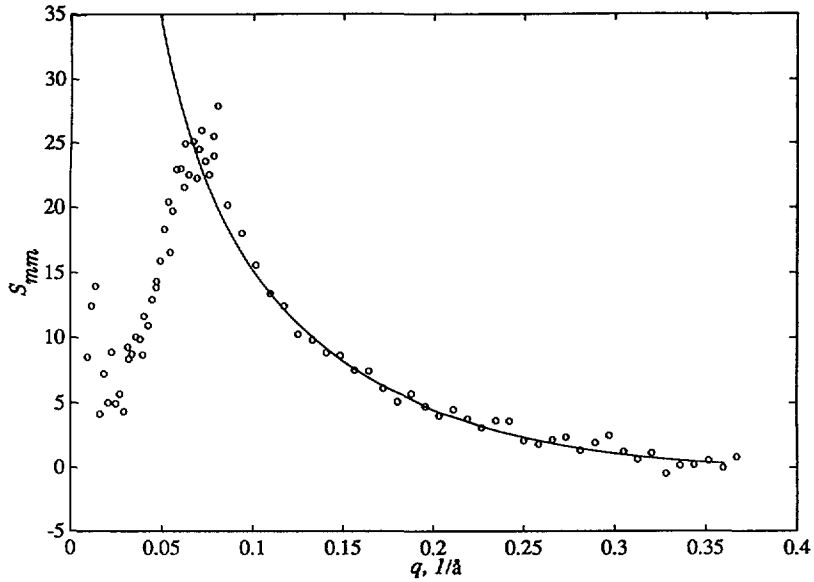

Fig. 5. — The monomer-monomer partial structure function S_{mm}. The solid curve represents the structure function of an uniform rod with L = 500 Å and r_p = 8 Å.

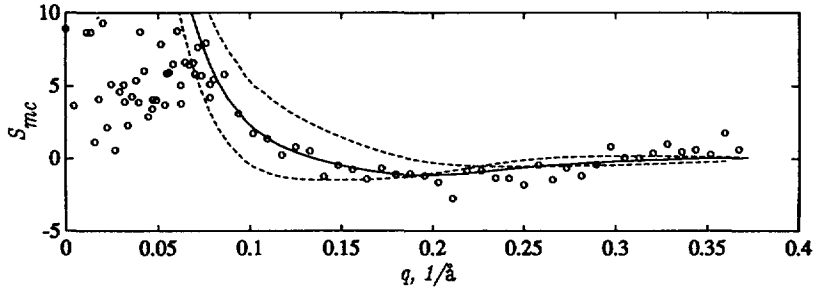

Fig. 6. — The monomer-counterion partial structure function S_{mc}. The solid curve is drawn according to the cell model calculation with r_p = 8 Å and r_c = 10, 14, and 18 Å from top to bottom. Note the minimum corresponding to a negative value of the structure function at a q value decreasing with r_c (for r_c = 14 Å : $q_{min} \approx 0.2$ Å^{-1}).

Due to electroneutrality, in the long wavelength limit ($q \to 0$) all three partial structure functions should tend to the thermodynamic limit. This limit is approximately ϕ^{-1}, ϕ being the osmotic coefficient [9]. The osmotic coefficient can be derived from the Poisson-Boltzmann equation with the cell model [8, 9]. Using the parameters collected in table I, one obtains $\phi^{-1} = 3.2$. This value agrees reasonably with the limiting behavior of the partial structure functions, despite the large experimental scatter in the low q range (Fig. 5-7).

The charge structure function can be evaluated using equation (5) and the partial structure functions obtained from samples s1, s3, and s4. This function is displayed in figure 8, together with the theoretical results using the cell model. The charge structure can also be obtained directly from the sample s2 data. After dividing by the appropriate scaling factor ($c\bar{b}^2$) the resulting structure function is also displayed in figure 8. In spite of the experimental

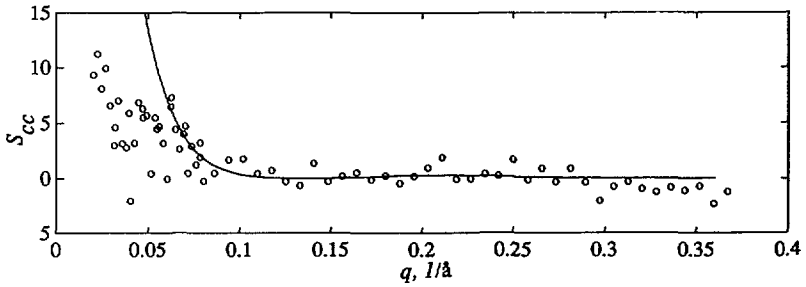

Fig. 7. — The counterion-counterion partial structure function S_{cc}. The solid curve is drawn according to the cell model calculation with $r_c = 14$ Å and $r_p = 8$ Å.

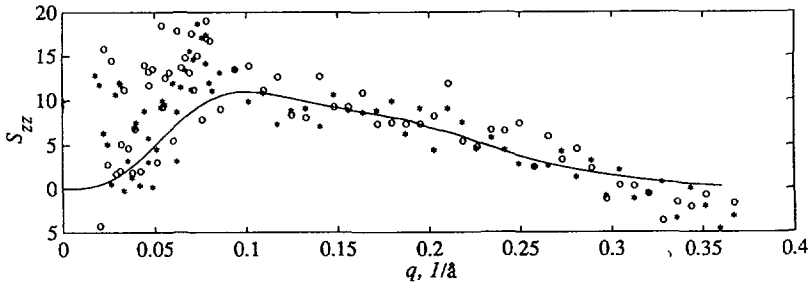

Fig. 8. — The charge structure function S_{zz}. (*) : directly measured (sample S2). (O) : derived from combination of partial structure functions according to equation (5). The solid curve is drawn according to the cell model calculation with $r_c = 14$ Å and $r_p = 8$ Å.

scatter, the two data sets are in reasonable agreement. This demonstrates the consistency of the data analysis and the presumed independence of the structure functions on the solvent isotopic composition. Since both experimental data sets are obtained in a statistically independent manner, they may be averaged. The result is displayed in figure 9.

The charge structure function (Fig. 9) shows reasonable agreement with the theoretical calculations using the Poisson-Boltzmann equation and the cell model. In fact, for this structure function, the agreement at small values of momentum transfer is much better than in case of the individual partial structure functions. This is due to a cancellation of intercellular effects. The radial charge density used to calculate the charge structure function is displayed in the inset of figure 9. The Stillinger-Lovett limiting law (Eq. (6)) is also displayed in figure 9. For small q values there is reasonable agreement taking a Debye screening length $\kappa^{-1} = 4 \pm 1$ nm. This length is somewhat larger than the characteristic decay distance of the counterion distribution as obtained from the solution of the Poisson-Boltzmann equation, 2.4 nm (see Fig. 9, inset).

The structure functions describing the interference between different cell volumes are experimentally estimated by subtracting the intracellular contribution from the experimental data (Fig. 10). In the small q range the intercellular structure functions deviate significantly from zero. It is clear that all three partial intercellular structure functions are similar. This indicates the strong coupling between the counterion atmosphere and the polyion. Furthermore, due to this similarity, intercellular effects cancel in the charge structure function. It is surprising that the transition « correlation distance » $q^{-1} \approx (1/0.05)$ Å is much shorter than

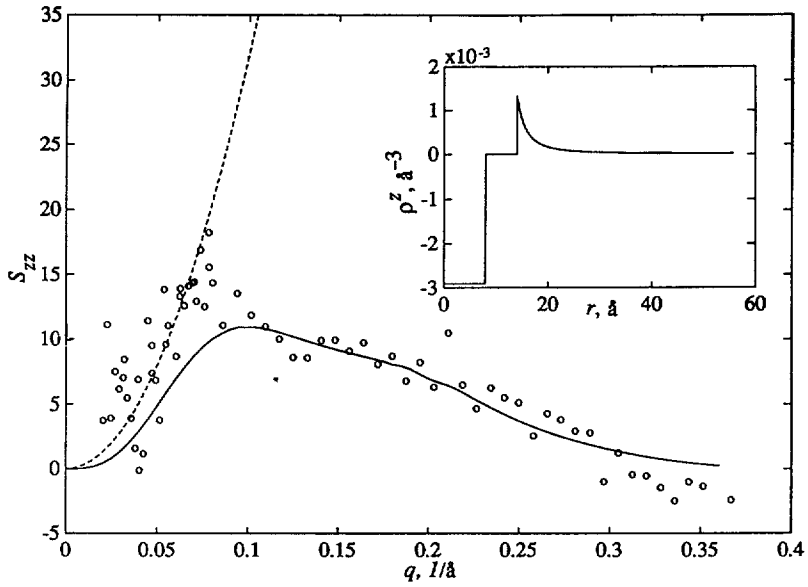

Fig. 9. — Charge structure function S_{zz} obtained from averaging the two independently derived charge structure functions displayed in figure 8. The solid curve is drawn according to the cell model calculation with $r_c = 14$ Å and $r_p = 8$ Å. The dashed curve represents the Stillinger-Lovett equation (6) with $\kappa^{-1} = 4$ nm. The inset shows the radial charge density used in the calculation.

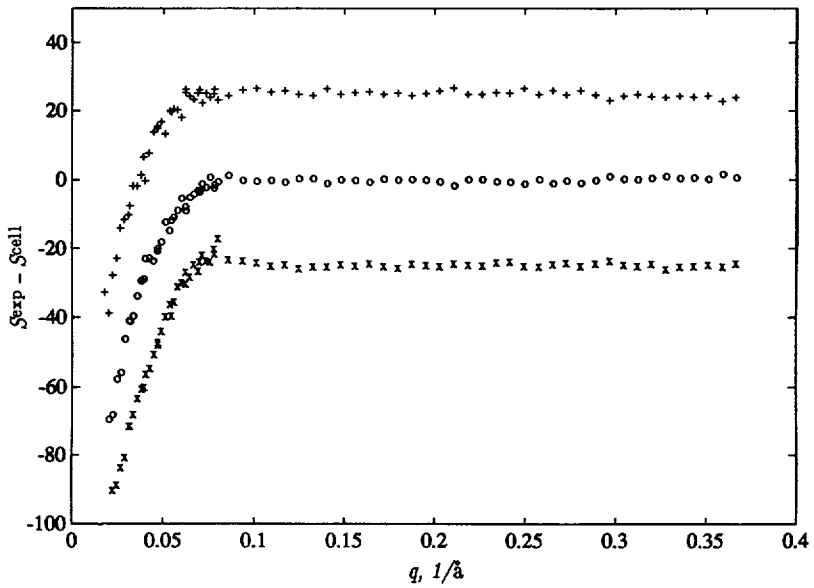

Fig. 10. — Structure functions describing the interference between different cell volumes. (+) : counterion-counterion (+ 25), (o) : monomer-counterion, (×) : monomer-monomer (– 25).

the cell radius r_{cell} = 55.8 Å. However, a detailed interpretation of these interference effects is difficult and beyond the scope of this contribution. In principle, it is possible to minimize the intercellular effects by performing experiments at lower DNA concentration. This will take considerable counting times, due to the weak scattering intensities.

5. Conclusions.

The data obtained in this experiment reflect in a direct manner the organization of the charges within the cell surrounding a single polyion. Several comments should be made about these results :

— The scattered intensities were measured in absolute units (cm^{-1}). The structure factors derived from the scattered intensities are scaled to absolute numbers : they have an intrinsic character.

— The reduction of the many chains problem to the single DNA cell in the analysis of the structure functions is found to agree with the observations made in the reciprocal space interval $q \geq 0.075$ Å^{-1} Conversely, the data below this value will reflect the organization among cells. This part of the data still needs to be interpreted.

— The partial structure functions and the charge structure function were interpreted using the charge distribution as obtained from the solution of the Poisson-Boltzmann equation in the cell model (see inset Fig. 9).

— The parameters r_p and r_c (polyion radius and distance of closest approach of the counterion to the rod) are used to adjust the calculated structure functions to the observed data in the range $q \geq 0.075$ Å^{-1}. The best fit is carried independently for *all* structure functions and yields the same set of values for r_p and r_c. The optimum value r_p = 8 Å is somewhat lower than the known outer DNA radius (10 Å, B-form [17]) : this is possibly due to the existence of grooves in the double helical structure. The counterion distance of closest approach r_c = 14 Å agrees reasonably with the sum of the outer polymer radius and the counterion radius (3.5 Å). The relatively bulky TMA counterions do not significantly penetrate into the DNA grooves. In a simple salt solution, the hydration of the TMA ion has been studied using the neutron diffraction first order difference method [18]. The TMA radial distribution functions show a relatively weak hydration structure in the range 3.5-5.5 Å. If the counterions reside near the phosphate moieties the short distance of closest approach does not allow intermediate hydration water. For fully hydrated counterions, the solvation sheaths can be accommodated by the DNA grooves. However, the present momentum transfer range does not allow a detailed analysis of the counterion short range structure.

— The counterion-counterion structure function S_{cc}, the cross correlation structure function S_{mc}, and the charge structure function S_{zz} contain the new information on the counterion radial distribution. The oscillation in $S_{mc}(q)$ reflects the accumulation of counterions near the polyion surface. The confinement within the cell is responsible for the slow decay of $S_{zz}(q)$ against $q \geq 0.075$ Å^{-1} It is also to be noticed that the expression of $S_{zz}(q)$ derived from the Poisson-Boltzmann equation and the cell model tends to zero in the long wavelength limit. This is due to the imposed electroneutrality of the cylindrical cell volume.

When using the Poisson-Boltzmann equation one should keep in mind the following. Short range interactions (including hydrophobic) as well as interactions between different polyions are neglected. The solvent is modeled as a continuum and the discrete size of the counterions is not taken into account. Furthermore, the true electrostatic potential is replaced by a potential of mean force. However, the merit of the present model is that it analytically describes the distribution of charges within an electroneutral cell. This distribution has been

successfully tested using the structure functions derived from the neutron scattering data. Other, perhaps more detailed, models describing the charge distribution [19] may be applied to these new experimental results.

Acknowledgments.

The authors thank J. C. Leyte, D. Bedeaux, C. W. A. Pley, P. Pfeuty, J. P. Cotton, and J. Noolandi for helpful discussions. L. Bezemer is gratefully acknowledged for help with the CD experiments.

Appendix.

In the cell model each molecule is thought to occupy a cylindrical cell volume. Interference effects between different cell volumes are explicitly neglected. Accordingly, the general expression of the structure functions reads

$$S_{ij}(q) = \frac{1}{N} \left\langle \int_{V_{\text{cell}}} \mathrm{d}\mathbf{r}\, \mathrm{e}^{-i\mathbf{q}\cdot\mathbf{r}}\, \rho_i(\mathbf{r}) \int_{V_{\text{cell}}} \mathrm{d}\mathbf{r}\, \mathrm{e}^{i\mathbf{q}\cdot\mathbf{r}}\, \rho_j(\mathbf{r}) \right\rangle_{\Omega} \tag{A1}$$

in which the integrations have to be performed over $\mathbf{r}$ in the total cell volume V_{cell}. The brackets denote an isotropic angular averaging of the cell with respect to the momentum vector $\mathbf{q}$. It is convenient to introduce cylindrical coordinates for the position vector $\mathbf{r}$. The position vector is given by the radial direction r, the projected longitudinal distance z and the azimuthal angle φ_r. The momentum transfer vector $\mathbf{q}$ is expressed in the spherical coordinates q, θ, and φ_q. Using these definitions, one has $\mathbf{q}\cdot\mathbf{r} = rq \sin(\theta)\cos(\varphi_r - \varphi_q) + qz\cos(\theta)$ and $\mathrm{d}\mathbf{r} = r\,\mathrm{d}r\,\mathrm{d}\varphi_r\,\mathrm{d}z$.

At a certain fixed cell orientation with respect to $\mathbf{q}$ (characterized by $\cos(\theta) = \mu$ and φ_q) the integral over $\mathbf{r}$ in the cell volume can be evaluated :

$$\int_{V_{\text{cell}}} \mathrm{d}\mathbf{r}\, \mathrm{e}^{-i\mathbf{q}\cdot\mathbf{r}}\, \rho_i(\mathbf{r}) = \int_{-L/2}^{L/2} \mathrm{d}z\, \mathrm{e}^{-iqz\mu} \int_0^{r_{\text{cell}}} \mathrm{d}r\, r\rho_i(r) \int_0^{2\pi} \mathrm{d}\varphi_r\, \mathrm{e}^{-iqr\cos(\varphi_r - \varphi_q)\sqrt{(1-\mu^2)}} \tag{A2}$$

The particle density is assumed to be uniform in the longitudinal direction and, hence, depends only on the radial coordinate r. The first and the last integral on the right hand side can be solved [20] :

$$\int_{V_{\text{cell}}} \mathrm{d}\mathbf{r}\, \mathrm{e}^{-i\mathbf{q}\cdot\mathbf{r}}\, \rho_i(\mathbf{r}) = \frac{\sin(q\mu L/2)}{(q\mu L/2)} P_i(q, \mu) \tag{A3}$$

with $P_i(q, \mu)$ given in equation (3b). The isotropic orientation averaging of the cell volume can readily be performed using

$$\langle .. \rangle_{\Omega} = \frac{1}{2\pi} \int_0^1 \mathrm{d}\mu \int_0^{2\pi} \mathrm{d}\varphi_q\, .. = \int_0^1 \mathrm{d}\mu\, . \tag{A4}$$

Inserting equation (A3) into equation (A1) together with the orientation averaging equation (A4) yields the desired expression equation (3).

Note added in proof :

In the cell model, the necessary conditions leading to the Stillinger-Lovett second sum rule are not fulfilled. Therefore, the first leading term in the expansion of the charge structure function is not proportional to q^2, but to q^4.

References

[1] NIERLICH M., BOUÉ F., LAPP A. and OBERTHUR R., *J. Phys. France* **46** (1985) 649 ; *Coll. Pol. Sci.* **263** (1985) 955.
[2] CHANG S.-L., CHEN S.-H., RILL R. L. and LIN J. S., *J. Phys. Chem.* **94** (1990) 8025.
[3] DERIAN P. J., BELLONI L. and DRIFFORD M., *Europhys. Lett.* **7** (1988) 243.
[4] JANNINK G., VAN DER MAAREL J. R. C., COTTON J. P., LAPP A., FARAGO B., LEYTE-ZUIDERWEG L. H. and with the collaboration of P. PFEUTY, unpublished results obtained at the institute Laue-Langevin and Laboratoire Léon-Brillouin. For earlier references, see NALLET F., JANNINK G., HAYTER J., OBERTHÜR R. and PICOT C., *J. Phys. France* **44** (1983) 87 and JANNINK G., *Makromol. Chem. Macromol. Symp.* **1** (1986) 67.
[5] NICOLAI T. and MANDEL M., *Macromolecules* **22** (1989) 2348.
[6] HAMAGUCHI K. and GEIDUSCHEK E. P., *J. Am. Chem. Soc.* **84** (1962) 1329.
[7] ALFREY T. Jr., BERG P. W. and MORAWETZ H., *J. Polym. Sci.* **7** (1951) 543.
[8] KATCHALSKY A., *J. Pure Appl. Chem.* **26** (1971) 327.
[9] MANDEL M., Encyclopedia of polymer science and engineering **11** (second Ed., John Wiley & Sons, Inc 1988) 739.
[10] JACROT B., *Rep. Prog. Phys.* **39** (1976) 911.
[11] DES CLOIZEAUX J. and JANNINK G., Polymers in solution. Their modelization and structure, Oxford university press (1990).
[12] HANSEN J.-P. and MCDONALD I. R., The theory of simple liquids (Academic Press New York, 1986).
[13] STILLINGER J. and LOVETT R., *J. Chem. Phys.* **49** (1968) 1991 ;
JANNINK G. and VAN DER MAAREL J. R. C., *Biophys. Chem.* **41** (1991) 15.
[14] VAN DIJK L., GRUWEL M. L. H., JESSE W., DE BLEIJSER J. and LEYTE J. C., *Biopolymers* **26** (1987) 261.
[15] HANLON S., BRUDNO S., WU T. T. and WOLF B., *Biochemistry* **14** (1975) 1648.
SAENGER W., Principles of nucleic acid structure (Springer New York, 1984).
[16] TERECH P., VOLINO F. and RAMASSEUL R., *J. Phys. France* **46** (1985) 895.
[17] MAHLER H. R. and CORDES E. H. Biological Chemistry (second Ed. Harper and Row New York, 1971).
[18] FINNEY J. L. and TURNER J., *Faraday Discuss. Chem. Soc.* **85** (1988) 1.
[19] LE BRET M. and ZIMM B. H., *Biopolymers* **23** (1984) 287.
[20] JAHNKE and EMDE, Table of functions (Dover publications, 1945).